The Dehydrogenation Mechanism and Reversibility of LiBH$_4$ Doped by Active Al Derived from AlH$_3$

Qing He [1,2], Dongdong Zhu [1], Xiaocheng Wu [2,*], Duo Dong [1], Xiaoying Jiang [1] and Meng Xu [1]

[1] Key Laboratory of Air-driven Equipment Technology of Zhejiang Province, Quzhou University, Quzhou 324000, China; helinqi@163.com (Q.H.); zhudd8@163.com (D.Z.); dongduohit@163.com (D.D.); qz_jxy1@163.com (X.J.); xmm2021@163.com (M.X.)

[2] Department of Materials Science and Engineering, Zhejiang University, Hangzhou 310058, China

[*] Correspondence: 11026032@zju.edu.cn; Tel.: +86-1356-700-5297

check for updates

Abstract: A detailed analysis of the dehydrogenation mechanism and reversibility of LiBH$_4$ doped by as-derived Al (denoted Al*) from AlH$_3$ was performed by thermogravimetry (TG), differential scanning calorimetry (DSC), mass spectral analysis (MS), powder X-ray diffraction (XRD), scanning electronic microscopy (SEM), and Fourier transform infrared spectroscopy (FTIR). The results show that the dehydrogenation of LiBH$_4$/Al* is a five-step reaction: (1) LiBH$_4$ + Al → LiH + AlB$_2$ + "Li-Al-B-H" + B$_2$H$_6$ + H$_2$; (2) the decomposition of "Li-Al-B-H" compounds liberating H$_2$; (3) 2LiBH$_4$ + Al → 2LiH + AlB$_2$ + 3H$_2$; (4) LiBH$_4$ → LiH + B + 3/2H$_2$; and (5) LiH + Al → LiAl + 1/2H$_2$. Furthermore, the reversibility of the LiBH$_4$/Al* composite is based on the following reaction: LiH + LiAl + AlB$_2$ + 7/2H$_2$ ↔ 2LiBH$_4$ + 2Al. The extent of the dehydrogenation reaction between LiBH$_4$ and Al* greatly depends on the precipitation and growth of reaction products (LiH, AlB$_2$, and LiAl) on the surface of Al*. A passivation shell formed by these products on the Al* is the kinetic barrier to the dehydrogenation of the LiBH$_4$/Al* composite.

Keywords: LiBH$_4$; Al; dehydrogenation mechanism; kinetic properties; reversibility

---

1. Introduction

Hydrogen is recognized as an ideal energy vector with the advantages of high combustion value and zero pollution [1–3]. However, the storage of hydrogen is still challenging for its on-board application. Hydrogen energy can be stored in gas, liquid, and solid forms, among which solid hydrogen storage is the safest. Currently, complex metal hydrides are considered as the most promising hydrogen storage materials due to their large hydrogen storage capacities [4–6].

Lithium borohydride (LiBH$_4$) has drawn much attention for on-board hydrogen storage due to its theoretical hydrogen storage capacity as high as 18.5 wt.%, which far exceeds the requirements of vehicle hydrogen storage material by the US department of energy [7,8]. Unfortunately, LiBH$_4$ is thermodynamically stable, and dehydrogenation is only initiated when the temperature is above 400 °C under 1 bar H$_2$. The reversibility of LiBH$_4$ is poor, and rehydrogenation requires a temperature over 600 °C under 350 bar H$_2$ [9,10]. Various methods have been developed to improve the dehydrogenation properties and reversibility of LiBH$_4$. Some researchers [11–13] found that thermodynamic destabilization of LiBH$_4$ could be achieved by adding reactive hydride composites (RHC) to change its dehydrogenation steps. For instance, Vajo et al. [13] reported that the dehydrogenation reaction enthalpy was much lower than that of the pure LiBH$_4$ by doping with MgH$_2$. The formation of MgB$_2$ during the dehydrogenation reaction destabilized LiBH$_4$, and the reversibility of the LiBH$_4$-MgH$_2$ composite was also better than pure LiBH$_4$. After that, many metal hydrides or complex hydrides have been employed to improve the hydrogen storage properties of LiBH$_4$ [14–21].

According to the theoretical calculation based on phase diagrams, the decomposition temperature of the LiBH$_4$/Al composite was predicted to be significantly lower than that of pure LiBH$_4$ [22,23]. Therefore, Al has been popularly employed as another destabilization agent to improve the hydrogen desorption properties of LiBH$_4$. The Al source can be either a metallic Al or a complex hydrides containing Al [24–26]. However, the metallic Al is usually coated with an oxide layer, which greatly limits the improvement of dehydrogenation and the reversibility of LiBH$_4$. Moreover, the utilization of Al-containing hydrides will inevitably introduce the influence of other atoms on the de/rehydrogenation reaction. In order to investigate the mechanism and influence of pure Al on the dehydrogenation and reversibility of LiBH$_4$, an as-prepared Al (denoted Al*) derived from AlH$_3$ was employed as a destabilization agent. The hydrogen desorption properties and mechanism of the LiBH$_4$/Al* composite were studied systematically, along with kinetic investigations using a Sieverts-type apparatus. The Kissinger method was used to calculate the activation energy of the main dehydrogenation step of the LiBH$_4$/Al* composite, and its reversibility was also discussed.

2. Materials and Methods

The LiBH$_4$ powder (95% purity; Acros Organics) and Al powder (99% purity; Sinopharm Group) were employed as raw materials. AlH$_3$ was synthesized as follows: LiAlH$_4$ and AlCl$_3$ were dissolved in diethyl ether at a molar ratio of 3:1. After the reaction (1) was fully carried out, the precipitate LiCl was filtered off, and the filtrate containing AlH$_3$ was separated from the mixture. Pure AlH$_3$ was then obtained from the filtrate by drying and de-ethering in vacuum. Finally, AlH$_3$ was completely dehydrogenated to obtain active Al* by heating to 200 °C and holding for 2.5 h. The dehydrogenation curves of AlH$_3$ and X-ray diffraction (XRD) patterns of AlH$_3$ before and after dehydrogenation are shown in Figure 1a,b, respectively.
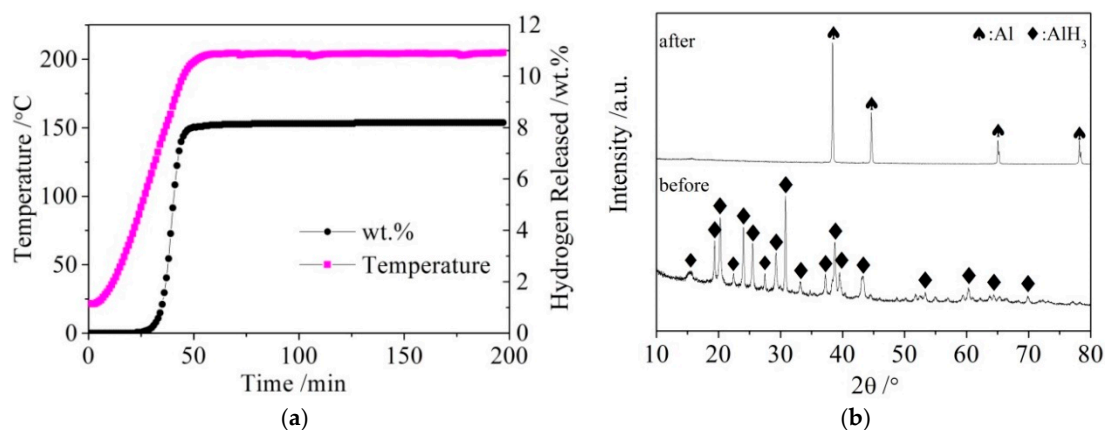
$$3LiAlH_4 + AlCl_3 \rightarrow 4AlH_3 + 3LiCl\downarrow \tag{1}$$

Figure 1. The dehydrogenation curves (**a**) of AlH$_3$ and X-ray diffraction (XRD) patterns (**b**) of AlH$_3$ before and after dehydrogenation.

The commercial Al powder was used for comparison with the as-prepared Al* in this study. The LiBH$_4$/Al and LiBH$_4$/Al* composites were synthesized by ball-milling using a QM-3SP4 planetary ball mill (Nanjing Nanda Instrument Plant, Nanjing, China). The ball to powder ratio was 45:1. The milling process was carried out at 400 rpm for 30 min under a 0.1 MPa argon atmosphere. To prevent the temperature from rising too fast during long-term milling, the milling process was paused every 6 min for cooling. All of the samples were handled in a Mikrouna glove box filled with high purity argon (99.999%) and controlled H$_2$O (<0.5 ppm) and O$_2$ (<0.1 ppm) concentrations for preventing contamination.

The morphologies of the as-received Al and as-prepared Al* were observed via field emission scanning electronic microscopy (SEM, Hitachi, Tokyo, Japan). Dehydriding/rehydriding behaviors of the samples were examined using a carefully calibrated Sieverts-type apparatus [27]. For the temperature programmed desorption (TPD) measurements, the samples were heated from room temperature to 600 °C at a rate of 2 °C/min. For the rehydriding measurements, the samples were heated to 400 °C at a rate of 5 °C/min under 8 MPa H_2 and held at that temperature for 7 h. The thermal events during dehydrogenation of the samples were investigated by thermogravimetry/differential scanning calorimeter (TG/DSC, Netzsch, Ahlden, Germany). For the isothermal hydrogen desorption measurements, the samples were rapidly heated to a set temperature (i.e., 100 °C, 350 °C, 500 °C, and 600 °C) and held for 3h under argon flowing at 50 mL/min. For the non-isothermal dehydrogenation (i.e., the temperature programmed desorption, TPD) measurements, the samples were heated gradually from room temperature to 600 °C with a heating rate of 5 °C/min. The hydrogen desorption spectra were collected synchronously using a mass spectrometer (MS, Netzsch, Ahlden, Germany). The phase of the as-prepared samples and the dehydrogenation product of them at various temperatures were identified by X-ray diffraction (XRD, PANalytical, Almelo, Netherlands) and Fourier transform infrared spectroscopy (FTIR, Bruker, Basel, Switzerland). During XRD measurements, the samples were sealed with a polypropylene membrane to avoid exposure to any moisture or oxygen.

3. Results and Discussion

3.1. Dehydrogenation Mechanism of the LiBH4/Al* Composite

The SEM images of the as-received Al particles and as-prepared Al* particles are shown in Figure 2. It can be seen that the particle size of the as-received Al is about 100 μm, while the particle size of active Al* derived from AlH_3 is about 1% of this. A sharp reduction in the particle size means a significant increase in the specific surface area.
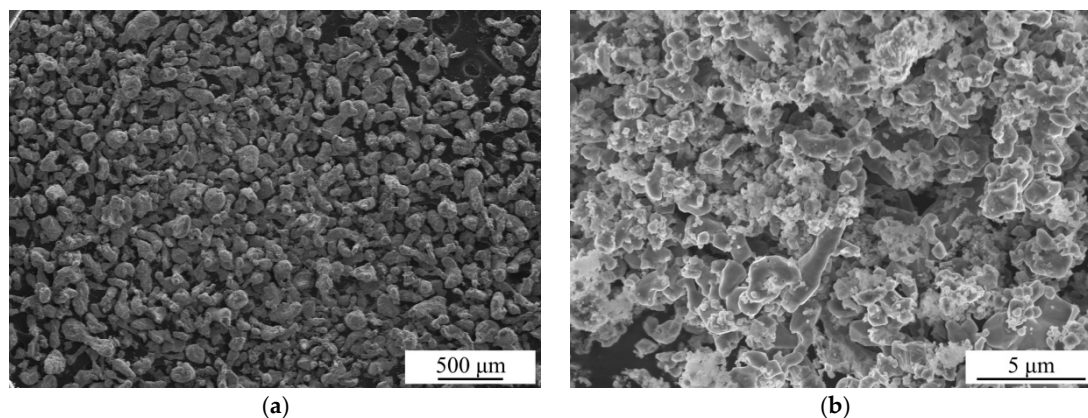

| (a) | (b) |

Figure 2. Scanning electronic microscopy (SEM) images of the as-received Al particles (**a**) and as-prepared Al* particles (**b**).

Figure 3 presents different simultaneous signals for the dehydrogenation of LiBH4/Al and LiBH4/Al* samples: the thermogravimetry (TG) signal, DSC signal, and hydrogen signal are plotted over the temperature. It can be seen from Figure 3a that the dehydrogenation curves of the LiBH4/Al and LiBH4/Al* composites are almost the same before 350 °C, and they both liberate about 0.1 wt.% of H_2. After being heated to 350 °C, the dehydrogenation rate of LiBH4/Al* is clearly faster than that of LiBH4/Al. Finally, the total dehydrogenation amounts of LiBH4/Al and LiBH4/Al* samples at 600 °C reached 5.5 wt.% and 6.2 wt.%, respectively. This can be ascribed to the Al* derived from AlH_3 having larger specific surface area, and the oxide-free surface of Al* possessing higher chemical reactivity. Therefore, the dehydrogenation reaction of LiBH4/Al* is more sufficient than LiBH4/Al.
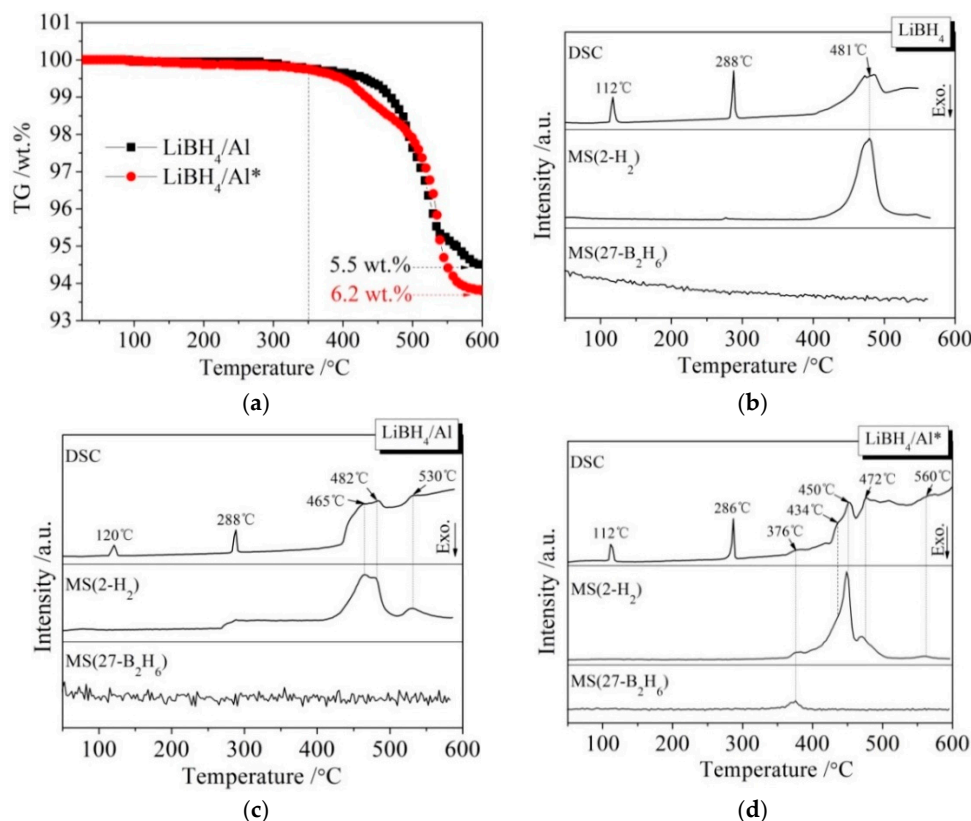
Figure 3. Thermogravimetry (TG) curves (**a**) of LiBH$_4$/Al and LiBH$_4$/Al* samples and differential scanning calorimetry/mass spectrometry (DSC/MS) curves of LiBH$_4$ (**b**), LiBH$_4$/Al (**c**), and LiBH$_4$/Al* (**d**) samples.

The DSC/MS curves of LiBH$_4$, LiBH$_4$/Al, and LiBH$_4$/Al* are displayed in Figure 3b–d, respectively. The endothermic peak in the DSC curve of pure LiBH$_4$ at 112 °C corresponds to the crystal transformation from an orthorhombic phase (o-LiBH$_4$) to a hexagonal phase (h-LiBH$_4$), while the endothermic peak at 288 °C corresponds to the melting of h-LiBH$_4$ [28]. LiBH$_4$ is dehydrogenated in the temperature range of 400 to 550 °C, and the dehydrogenation rate reached a maximum at 481 °C according to Figure 3b. Therefore, the endothermic peak at this temperature is ascribed to the decomposition of LiBH$_4$ based on Reaction (2).

$$LiBH_4 \rightarrow LiH + B + 3/2H_2\uparrow \tag{2}$$

There are three endothermic peaks at 465, 482, and 530 °C in the DSC curve of the LiBH$_4$/Al sample (Figure 3c). Each endothermic peak corresponds to a hydrogen evolution peak in the MS curve. The endothermic peak at 482 °C is in good agreement with that of the decomposition of LiBH$_4$ mentioned above. Compared with Figure 3b, the new endothermic peaks at 465 and 530 °C should be related to the reaction of LiBH$_4$ and the added Al. According to the work of other researchers [29–31], the endothermic peak at 465 °C is ascribed to the LiBH$_4$ reaction with Al forming LiH, AlB$_2$, and liberating H$_2$ (Reaction (3)), and the endothermic peak at 530 °C is attributed to the reaction of LiH with Al to form LiAl alloy and H$_2$ (Reaction (4)).

$$2LiBH_4 + Al \rightarrow 2LiH + AlB_2 + 3H_2\uparrow \tag{3}$$

$$LiH + Al \rightarrow LiAl + 1/2H_2\uparrow \tag{4}$$
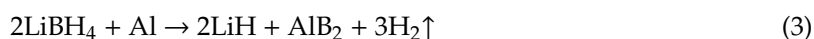
It can be seen from Figure 3d that the dehydrogenation behavior of LiBH$_4$/Al* is more sophisticated than that of LiBH$_4$/Al. There is a tiny endothermic peak appearing at 376 °C in the DSC curve of the LiBH$_4$/Al* composite, accompanied by a small amount of H$_2$ and B$_2$H$_6$ desorption reflected in the MS

curve. What is more, there are four endothermic peaks of dehydrogenation locate at 434, 450, 472, and 560 °C. In order to investigate the mechanism of these thermal events, XRD and FTIR analyses were conducted on the solid products of the $LiBH_4$/Al* sample at different dehydrogenation temperatures (e.g., 100, 350, 500, and 600 °C). The results are shown in Figure 4; Figure 5, respectively. It can be seen from Figure 4a that no new phase was detected when the sample was heated to 100 °C. The shrinkage of the diffraction peaks of $LiBH_4$ is related to its crystal transformation. When the sample was heated to 350 °C, some tiny diffraction peaks of AlB_2 and an unknown phase appeared. The unknown phase, marked "?", was also reported by other researchers and considered to be compounds with components of Li-Al-B [32,33]. Combined with the FTIR spectra in Figure 5a, the diffraction peaks of LiH overlapping with the diffraction peaks of Al can also be found in Figure 4a at this stage. This indicates that $LiBH_4$ had started to react with Al* to form LiH, AlB_2, and compounds containing Li-Al-B. At the same time, B_2H_6 and H_2 were released, and the rate reached a peak at 376 °C according to Figure 3d. Therefore, the further decrease of the diffraction intensity of $LiBH_4$ at 350 °C (Figure 4a) can be attributed to its melting and dehydrogenation. When the sample was heated to 500 °C, the $LiBH_4$ could not be detected by the XRD analysis (Figure 4a), and the vibrational peaks of B–H stretching (2382, 2292, and 2224 cm^{-1}) and bending (1125 cm^{-1}) disappeared (Figure 5a), indicating that $LiBH_4$ had been completely consumed in dehydrogenation reactions at 376, 434, 450, and 472 °C (Figure 3d). What is more, the diffraction peaks of LiAl appeared, and the diffraction intensity of LiH and AlB_2 slightly increased, while the peaks of Al weakened, and the peaks of compounds containing Li-Al-B disappeared. Combined with the analyses of $LiBH_4$ and $LiBH_4$/Al samples, it can be reasonably assumed that the main dehydrogenation peak of $LiBH_4$/Al* at 450 °C is attributed to the reaction of $LiBH_4$ and Al to form LiH, AlB_2, and H_2 based on Reaction (3). The reaction temperature was lower than that of the $LiBH_4$/Al sample probably because the particle size of active Al* derived from AlH_3 is much smaller than that of as-purchased Al, and the oxide-free surface of Al* possesses higher chemical reactivity. An easier atomic diffusion and shorter diffusion lengths led to less activation energy required for the reaction. The dehydrogenation peak at 472 °C is ascribed to the self-decomposition of $LiBH_4$ forming LiH, B, and H_2 based on Reaction (2). However, the diffraction peaks of B were not found in the XRD examination, and this may be because B was in an amorphous state. Therefore, the dehydrogenation peak at 434 °C is probably related to the decomposition of the unknown compounds, which can be denoted as "Li-Al-B-H". Furthermore, the dehydrogenation peak at 376 °C is believed to be attributed to Reaction (5). In addition, AlB_2 is generally considered to be a product that makes the dehydrogenation system reversible, while B_2H_6 is a toxic gas, which may be a problem for the future application of the $LiBH_4$/Al* system. Finally, the appearance of LiAl indicates that LiH had begun to react with Al* to form LiAl and liberate H_2 (Reaction (4)) before 500 °C.
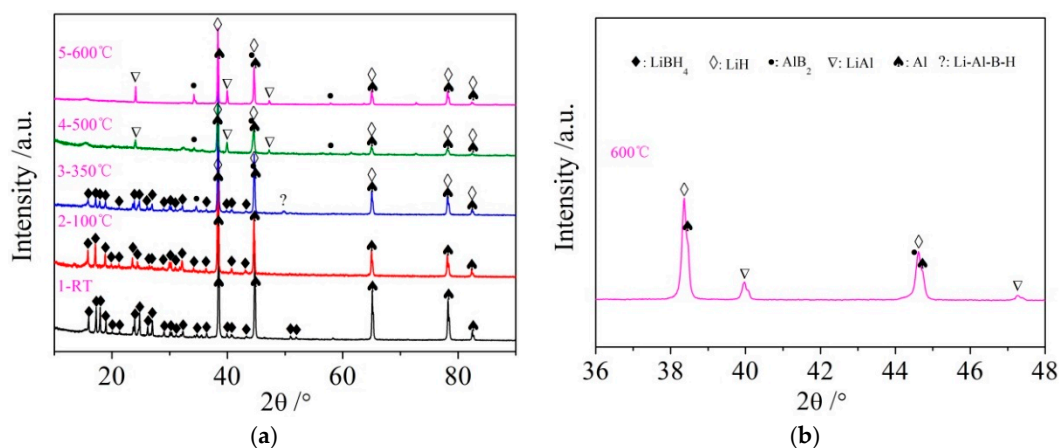
$$LiBH_4 + Al \rightarrow LiH + AlB_2 + \text{"Li-Al-B-H"} + B_2H_6\uparrow + H_2\uparrow \tag{5}$$
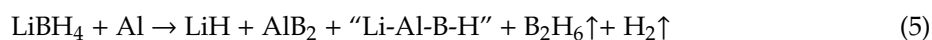
Figure 4. XRD patterns (**a**) of the LiBH$_4$/Al* sample obtained at different temperatures (room temperature, 100, 350, 500, and 600 °C) and expanded XRD pattern of LiBH$_4$/Al* sample of 600 °C at a 2θ range of 36–48° (**b**).

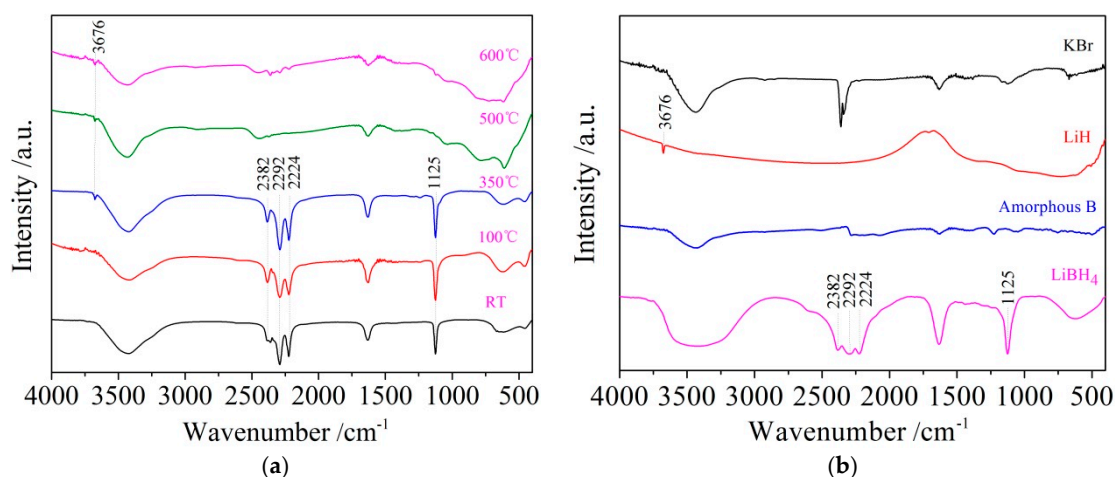**Figure 5.** Fourier transform infrared spectroscopy (FTIR) patterns of the LiBH$_4$/Al* sample (**a**) obtained at different temperatures (room temperature, 100, 350, 500, and 600 °C) and reference substances (**b**) including KBr, LiH, amorphous B, and LiBH$_4$.

Compared with the XRD patterns at 500 °C, no new phase was detected when the LiBH$_4$/Al* sample was heated to 600 °C. The increase of the relative diffraction intensity of LiAl implies that the reaction of LiH with Al* continued from 500 to 600 °C. The dehydrogenation rate of this reaction reached a peak at 560 °C according to Figure 3d. The existence of LiH and Al suggests that the LiBH$_4$/Al* system still dehydrogenated incompletely even at 600 °C. In fact, the dehydrogenation amount of the LiBH$_4$/Al* sample is far from the theoretical value (7.2 wt.%) according to Figure 3a, indicating that there exist some kinetic barriers in the dehydrogenation reaction of the LiBH$_4$/Al* composite. Moreover, the physical barrier is probably the reaction products from the previous step, which surround the Al* particles and preventing Al* from coming into contact with other reactants.

The whole hydrogen desorption process of the LiBH$_4$/Al* sample, which is schematically shown in Figure 6, can be concluded as follows: While heating in the crucible, LiBH$_4$ first transformed from an orthorhombic phase (*o*-LiBH$_4$) to a hexagonal phase (*h*-LiBH$_4$) at 112 °C and melted at 288 °C. Then, the molten LiBH$_4$ reacted with Al* to form LiH, AlB$_2$, and "Li-Al-B-H" compounds while releasing B$_2$H$_6$ and H$_2$ based on Reaction (5) at 376 °C. As the LiH, AlB$_2$, and "Li-Al-B-H" compounds were supposed to nucleate and grow on the surface of Al*, the reaction stopped when Al* was completely wrapped by these reaction products to form a passivation shell. When the temperature rose to 434 °C, the decomposition of the "Li-Al-B-H" compounds liberated a certain amount of H$_2$, and the

encapsulated Al* exposed some new surfaces. Thus, the main dehydrogenation reaction of LiBH$_4$ and Al* occurred at 450 °C to form LiH, AlB$_2$, and H$_2$ based on reaction (3). Similarly, the reaction stopped when the surface of Al* was completely wrapped by LiH and AlB$_2$. Therefore, the excess molten LiBH$_4$ underwent self-decomposition to form LiH, B, and H$_2$ (Reaction (2)) at 472 °C. That boron (B) was not detected in the XRD examination may be because B was in the amorphous state. Finally, the product LiH reacted with Al* to form LiAl alloy and H$_2$ based on Reaction (4) when the sample was heated to 560 °C. The actual dehydrogenation amount of the LiBH$_4$/Al* sample did not reach the theoretical value since there were still uncontacted and unreacted LiH and Al* at 600 °C.
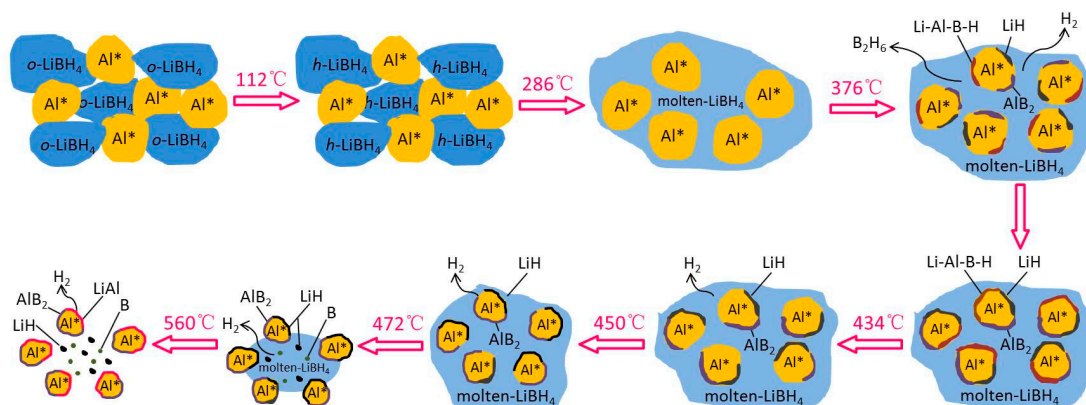

Figure 6. Schematic diagram of the dehydrogenation process of the LiBH$_4$/Al* sample.

3.2. Kinetic Properties of the Dehydrogenation of the LiBH$_4$/Al* Composite

The kinetic properties of the dehydrogenation of the LiBH$_4$/Al* composite were studied using the Kissinger method, which assumes that the apparent activation energy (E_a) of dehydrogenation reaction is determined by Equation (6).

$$\ln(\beta/T_m{}^2) = -E_a/RT_m + C \tag{6}$$

In this equation, β is the heating rate in thermal analysis, and T_m represents the absolute temperature at the maximum reaction rate. Moreover, R is the universal gas constant, and C also represents a constant. Therefore, the E_a of the dehydrogenation reaction of the LiBH$_4$/Al* composite can be obtained from the slope of a linearly fitted line in the $\ln(\beta/T_m{}^2)$-$T_m{}^{-1}$ spectrum.

During the kinetic investigations, the LiBH$_4$/Al and LiBH$_4$/Al* samples were heated to 600 °C at the rates of 5, 10, and 20 °C/min, respectively. The MS curves at various heating rates and the Kissinger spectra reflecting the E_a of the main dehydrogenation reaction are shown in Figure 7. It can be seen that the temperatures for the maximum dehydrogenation rate of LiBH$_4$/Al* at the heating rates of 5, 10, and 20 °C/min are 449.9, 471.1, and 485.2 °C, respectively. These are all lower than that of LiBH$_4$/Al at the same heating rates. The E_a of the main dehydrogenation reaction of LiBH$_4$/Al* is calculated to be 163.8 kJ/mol, while that of LiBH$_4$/Al is 243.5 kJ/mol. This is in good agreement with the previous analysis that the smaller particle size and higher chemical reactivity of Al* can reduce the activation energy and improve the kinetic properties of the dehydrogenation reaction.
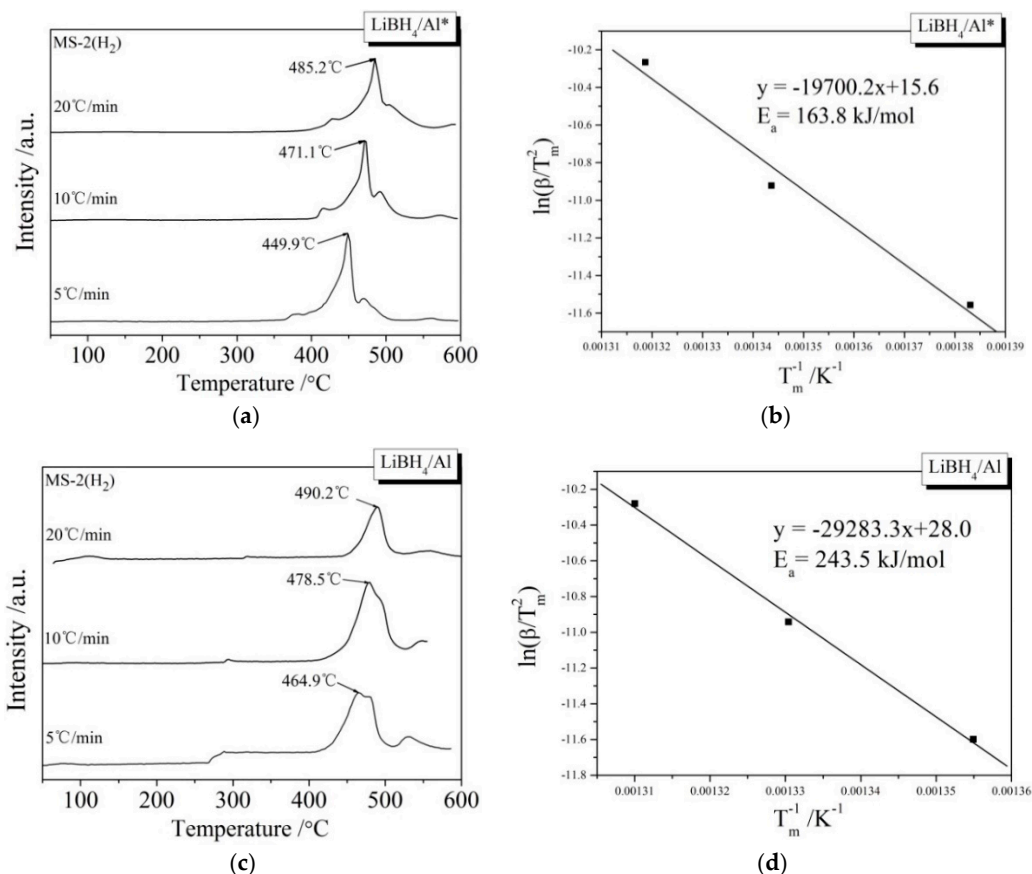
Figure 7. MS curves (**a**,**c**) of LiBH$_4$/Al* and LiBH$_4$/Al samples at different heating rates (5, 10, and 20 °C/min) and Kissinger spectra (**b**,**d**) of the main dehydrogenation reaction of the LiBH$_4$/Al* and LiBH$_4$/Al samples.

3.3. Reversibility of the LiBH$_4$/Al* Composite

In order to investigate the reversibility of the LiBH$_4$/Al* composite, a rehydrogenation test was carried out under 8 MPa H$_2$ at 400 °C. The rehydrogenation curve of the sample is shown in Figure 8. It can be seen that the dehydrogenated LiBH$_4$/Al* sample absorbed 2.6 wt.% of hydrogen in the first 60 min. Then it entered a stable hydrogen absorption stage and reached saturation after 480 min. The total rehydrogenation capacity was 5.5 wt.%. Compared with the harsh rehydrogenation conditions reported by other researchers [9,10], the doping of active Al* derived from AlH$_3$ effectively improved the reversible hydrogen storage properties of LiBH$_4$.
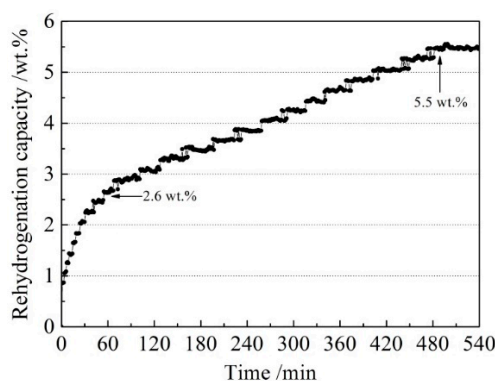

Figure 8. The rehydrogenation curve of the dehydrogenated LiBH$_4$/Al* sample under 8 MPa H$_2$ at 400 °C.

The rehydrogenation mechanism exploration was conducted using XRD and FTIR analysis of the rehydrided products of the LiBH$_4$/Al* sample, and the results are shown in Figure 9a,b, respectively. It can be seen from the XRD patterns that the diffraction peaks of LiAl, LiH, and AlB$_2$ disappeared, while the diffraction peaks of LiBH$_4$ reappeared, and the diffraction intensity of Al increased after rehydrogenation. Furthermore, the vibrational peaks of B–H stretching (2382, 2292, and 2224 cm^{-1}) and bending (1125 cm^{-1}) were also detected in the FTIR spectra. Therefore, the re-formation of LiBH$_4$ can be confirmed during the rehydrogenation process. Based on the above analysis, it can be safely concluded that the rehydrogenation process of LiBH$_4$/Al* is based on Reaction (7).
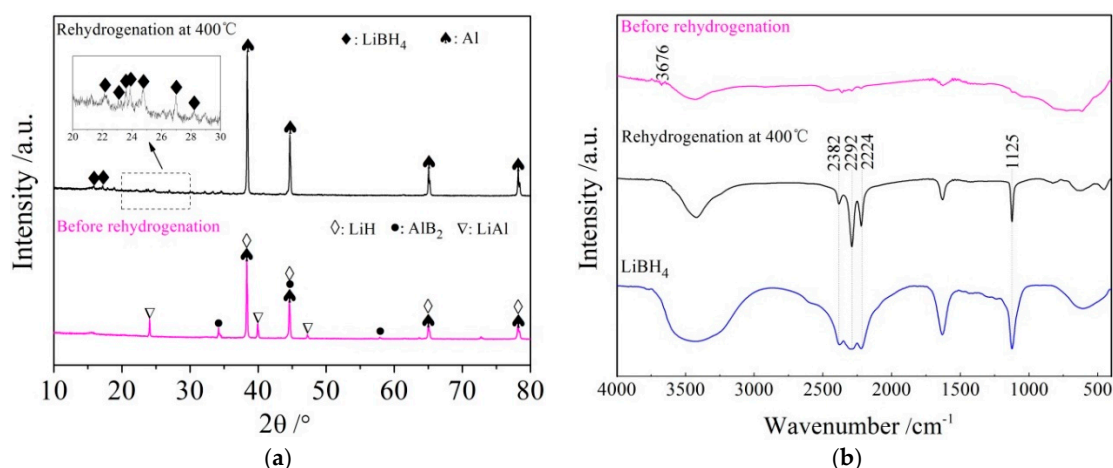
$$\text{LiH + LiAl + AlB}_2 + 7/2\text{H}_2 \leftrightarrow 2\text{LiBH}_4 + 2\text{Al} \tag{7}$$

Figure 9. XRD patterns (**a**) and FTIR spectra (**b**) of LiBH$_4$/Al* sample before and after rehydrogenation.

4. Conclusions

The dehydrogenation of LiBH$_4$ doped by active Al* derived from AlH$_3$ results from a five-step reaction: (1) LiBH$_4$ + Al → LiH + AlB$_2$ + "Li-Al-B-H" + B$_2$H$_6$ + H$_2$; (2) the decomposition of "Li-Al-B-H" compounds liberating H$_2$; (3) 2LiBH$_4$ + Al → 2LiH + AlB$_2$ + 3H$_2$; (4) LiBH$_4$ → LiH + B + 3/2H$_2$; and (5) LiH + Al → LiAl + 1/2H$_2$. Furthermore, the reversibility of the LiBH$_4$/Al* composite is based on the following reaction: LiH + LiAl + AlB$_2$ + 7/2H$_2$ ↔ 2LiBH$_4$ + 2Al.

The hydrogen desorption kinetics of LiBH$_4$ were effectively improved by doping with active Al* derived from AlH$_3$. Higher dehydrogenation capacity, lower activation energy, and better reversibility of LiBH$_4$/Al* can be achieved due to the larger specific surface area and higher chemical reactivity of Al*. The extent of the dehydrogenation reaction between LiBH$_4$ and Al* greatly depended on the precipitation and growth of reaction products (LiH, AlB$_2$, and LiAl) on the surface of the Al*. A passivation shell formed by these products on the Al* is the kinetic barrier to the dehydrogenation of the LiBH$_4$/Al* composite. Therefore, future work should focus on cracking this barrier to further improve the hydrogen storage properties of the LiBH$_4$/Al* composite.

Author Contributions: Conceptualization, Q.H. and D.Z.; methodology, Q.H. and D.D.; data curation, M.X. and X.W.; formal analysis, X.W.; investigation, M.X. and X.J.; resources, Q.H.; supervision, Q.H.; project administration, Q.H.; funding acquisition, Q.H.; writing-original draft preparation, X.W.; writing-review and editing, Q.H. and D.Z.

Conflicts of Interest: The authors declare no conflict of interest.

References

1.　Parra, D.; Valverde, L.; Pino, F.J.; Patel, M.K. A review on the role, cost and value of hydrogen energy systems for deep decarbonisation. *Renew. Sustain. Energy Rev.* **2019**, *101*, 279–294. [CrossRef]

2.　Colbertaldo, P.; Agustin, S.B.; Campanari, S.; Brouwer, J. Impact of hydrogen energy storage on California electric power system: Towards 100% renewable electricity. *Int. J. Hydrogen Energy* **2019**, *44*, 9558–9576. [CrossRef]

3.　Zhao, G.; Nielsen, E.R.; Troncoso, E.; Hyde, K.; Romeo, J.S.; Diderich, M. Life cycle cost analysis: A case study of hydrogen energy application on the Orkney Islands. *Int. J. Hydrogen Energy* **2019**, *44*, 9517–9528. [CrossRef]

4.　Orimo, S.I.; Nakamori, Y.; Eliseo, J.R.; Züttel, A.; Jensen, C.M. Complex hydrides for hydrogen storage. *Chem. Rev.* **2007**, *107*, 4111–4132. [CrossRef]

5.　Milanese, C.; Jensen, T.R.; Hauback, B.C.; Pistidda, C.; Dornheim, M.; Yang, H.; Lombardo, L.; Zuettel, A.; Filinchuk, Y.; Ngene, P.; et al. Complex hydrides for energy storage. *Int. J. Hydrogen Energy* **2019**, *44*, 7860–7874. [CrossRef]

6.　Puszkiel, J.; Garroni, S.; Milanese, C.; Gennari, F.; Klassen, T.; Dornheim, M.; Pistidda, C. Tetrahydroborates: Development and potential as hydrogen storage medium. *Inorganics* **2017**, *5*, 74. [CrossRef]

7.　Wu, R.; Ren, Z.; Zhang, X.; Lu, Y.; Li, H.; Gao, M.; Pan, H.; Liu, Y. Nanosheet-like Lithium Borohydride Hydrate with 10 wt.% of Hydrogen Release at 70 °C as a Chemical Hydrogen Storage Candidate. *J. Phys. Chem. Lett.* **2019**, *10*, 1872–1877. [CrossRef]

8.　*DOE, U.S. Targets for Onboard Hydrogen Storage Systems for Light-Duty Vehicles*; US Department of Energy, Office of Energy Efficiency and Renewable Energy and The Freedom CAR and Fuel Partnership: Washington, DC, USA, 2009.

9.　Orimo, S.I.; Nakamori, Y.; Kitahara, G.; Miwa, K.; Ohba, N.; Towata, S.I.; Züttel, A. Dehydriding and rehydriding reactions of $LiBH_4$. *J. Alloys Compd.* **2005**, *404*, 427–430. [CrossRef]

10.　Liu, X.; Peaslee, D.; Jost, C.Z.; Baumann, T.F.; Majzoub, E.H. Systematic pore-size effects of nanoconfinement of $LiBH_4$: Elimination of diborane release and tunable behavior for hydrogen storage applications. *Chem. Mater.* **2011**, *23*, 1331–1336. [CrossRef]

11.　Paskevicius, M.; Jepsen, L.H.; Schouwink, P.; Černý, R.; Ravnsbæk, D.B.; Filinchuk, Y.; Dornheim, M.; Besenbacher, F.; Jensen, T.R. Metal borohydrides and derivatives-synthesis, structure and properties. *Chem. Soc. Rev.* **2017**, *46*, 1565–1634. [CrossRef]

12.　Von Colbe, J.B.; Ares, J.R.; Barale, J.; Baricco, M.; Buckley, C.; Capurso, G.; Gallandat, N.; Grant, D.; Guzik, M.; Jacob, I.; et al. Application of hydrides in hydrogen storage and compression: Achievements, outlook and perspectives. *Int. J. Hydrogen Energy* **2019**, *44*, 7780–7808. [CrossRef]

13.　Vajo, J.J.; Skeith, S.L.; Mertens, F. Reversible storage of hydrogen in destabilized $LiBH_4$. *J. Phys. Chem. B* **2005**, *109*, 3719–3722. [CrossRef]

14.　Chaudhary, A.L.; Li, G.; Matsuo, M.; Orimo, S.I.; Deledda, S.; Sørby, M.H.; Hauback, B.C.; Pistidda, C.; Klassen, T.; Dornheim, M. Simultaneous desorption behavior of M borohydrides and Mg_2FeH_6 reactive hydride composites (M = Mg, then Li, Na, K, Ca). *Appl. Phys. Lett.* **2015**, *107*, 073905. [CrossRef]

15.　Puszkiel, J.A.; Gennari, F.C. Reversible hydrogen storage in metal-doped Mg-$LiBH_4$ composites. *Scr. Mater.* **2009**, *60*, 667–670. [CrossRef]

16.　Mao, J.F.; Guo, Z.P.; Liu, H.K.; Yu, X.B. Reversible hydrogen storage in titanium-catalyzed $LiAlH_4$-$LiBH_4$ system. *J. Alloys Compd.* **2009**, *487*, 434–438. [CrossRef]

17.　Puszkiel, J.A.; Gennari, F.C.; Larochette, P.A.; Ramallo-López, J.M.; Vainio, U.; Karimi, F.; Pranzas, P.K.; Troiani, H.; Pistidda, C.; Jepsen, J.; Tolkiehn, M.; et al. Effect of Fe additive on the hydrogenation-dehydrogenation properties of $2LiH + MgB_2/2LiBH_4+MgH_2$ system. *J. Power Sources* **2015**, *284*, 606–616. [CrossRef]

18.　Noritake, T.; Aoki, M.; Towata, S.; Ninomiya, A.; Nakamori, Y.; Orimo, S. Crystal structure analysis of novel complex hydrides formed by the combination of $LiBH_4$ and $LiNH_2$. *Appl. Phys. A* **2006**, *83*, 277–279. [CrossRef]

19.　Shi, Q.; Yu, X.; Feidenhans'l, R.; Vegge, T. Destabilized $LiBH_4$-$NaAlH_4$ Mixtures Doped with Titanium Based Catalysts. *J. Phys. Chem. C* **2008**, *112*, 18244–18248. [CrossRef]

20. Sofianos, M.V.; Chaudhary, A.L.; Paskevicius, M.; Sheppard, D.A.; Humphries, T.D.; Dornheim, M.; Buckley, C.E. Hydrogen storage properties of eutectic metal borohydrides melt-infiltrated into porous Al scaffolds. *J. Alloys Compd.* **2019**, *775*, 474–480. [CrossRef]

21. Zhang, Y.; Tian, Q. The reactions in $LiBH_4$-$NaNH_2$ hydrogen storage system. *Int. J. Hydrogen Energy* **2011**, *36*, 9733–9742. [CrossRef]

22. Jiang, W.; Cao, S. Effect of Al on the dehydrogenation of $LiBH_4$ from first-principles calculations. *Int. J. Hydrogen Energy* **2017**, *42*, 6181–6188.

23. Cho, Y.W.; Shim, J.H.; Lee, B.J. Thermal destabilization of binary and complex metal hydrides by chemical reaction: A thermodynamic analysis. *Calphad* **2006**, *30*, 65–69. [CrossRef]

24. Yu, X.; Xia, G.; Guo, Z.; Liu, H. Dehydrogenation/rehydrogenation mechanism in aluminum destabilized lithium borohydride. *Int. J. Mater. Res.* **2009**, *24*, 2720–2727. [CrossRef]

25. Kato, S.; Bielmann, M.; Ikeda, K.; Orimo, S.I.; Borgschulte, A.; Züttel, A. Surface changes on AlH_3 during the hydrogen desorption. *Appl. Phys. Lett.* **2010**, *96*, 051912. [CrossRef]

26. Carrillo-Bucio, J.; Tena-García, J.; Suárez-Alcántara, K. Dehydrogenation of surface-oxidized mixtures of $2LiBH_4$+ Al/Additives (TiF_3 or CeO_2). *Inorganics* **2017**, *5*, 82. [CrossRef]

27. Kwak, Y.J.; Song, M.Y. How to Analyse Metal Hydride Decomposition Temperatures Using a Sieverts' Type Hydriding-Dehydriding Apparatus and Hydrogen-Storage Characteristics for an MgH_2-Based Alloy. *Mater. Sci.* **2018**, *24*, 24–28. [CrossRef]

28. Züttel, A.; Rentsch, S.; Fischer, P.; Wenger, P.M.C.E.P.; Sudan, P.H.; Mauron, P.; Emmenegger, C. Hydrogen storage properties of $LiBH_4$. *J. Alloys Compd.* **2003**, *356*, 515–520. [CrossRef]

29. Kang, X.D.; Wang, P.; Ma, L.P.; Cheng, H.M. Reversible hydrogen storage in $LiBH_4$ destabilized by milling with Al. *Appl. Phys. A* **2007**, *89*, 963–966. [CrossRef]

30. Zhang, Y.; Tian, Q.; Zhang, J.; Liu, S.S.; Sun, L.X. The dehydrogenation reactions and kinetics of $2LiBH_4$-Al composite. *J. Phys. Chem. C* **2009**, *113*, 18424–18430. [CrossRef]

31. Friedrichs, O.; Kim, J.W.; Remhof, A.; Buchter, F.; Borgschulte, A.; Wallacher, D.; Cho, Y.W.; Fichtner, M.; Ohb, K.H.; Züttel, A. The effect of Al on the hydrogen sorption mechanism of $LiBH_4$. *Phys. Chem. Chem. Phys.* **2009**, *11*, 1515–1520. [CrossRef]

32. Plerdsranoy, P.; Utke, R. Confined $LiBH_4$-$LiAlH_4$ in nanopores of activated carbon nanofibers. *Int. J. Hydrogen Energy* **2015**, *40*, 7083–7092. [CrossRef]

33. Hansen, B.R.; Ravnsbæk, D.B.; Reed, D.; Book, D.; Gundlach, C.; Skibsted, J.; Jensen, T.R. Hydrogen storage capacity loss in a $LiBH_4$-Al composite. *J. Phys. Chem. C* **2013**, *117*, 7423–7432. [CrossRef]